International Journal of Engineering Science Invention
ISSN (Online): 2319 – 6734, ISSN (Print): 2319 – 6726
www.ijesi.org ||Volume 6 Issue 9|| September 2017 || PP. 71-76

Optical Properties of Molecule-Like Au_{25} Nanoparticles

Amit Patel, Michael C. On, Jai-Pil Choi*
Department of Chemistry, California State University – Fresno, 2555 East San Ramon Avenue, M/S SB70, Fresno, California 93740, United States of America
Corresponding Author: Jai-Pil Choi

Abstract: *This paper describes the effect of solvent polarity on the optical properties of molecule-like Au_{25} nanoparticles. UV-Vis absorption and photoluminescence were measured using various organic solvents (aromatic vs. non-aromatic). The molar extinction coefficients and the relative quantum efficiency of Au_{25} were determined and correlated with the normalized empirical parameters of solvent polarity. The molar extinction was linearly decreased as increasing solvent polarity, but the relative quantum efficiency was significantly affected by aromatic solvent only. The HOMO-LUMO energy gap (1.32 – 1.33 eV) estimated from absorption band edges was not influenced by solvent polarity. However, the measured relative quantum efficiency was varied from 7.6×10^{-3} to 20.4×10^{-3}, depending on solvent polarity as well as the excitation wavelength.*

Keywords: *Absorption, Gold Nanoparticles, Molar Extinction, Photoluminescence, Quantum Efficiency*

Date of Submission: 26-08-2017 Date of acceptance: 09-09-2017

I. INTRODUCTION

Nanomaterials have attracted widespread interest in research and development, because they are a new group of materials displaying the different properties from their individual atoms as well as their bulk counter-parts. It has been well known that the physicochemical properties of nanomaterials can be affected by their size [1-5], shape [2-4], and composition [3]. The advent of new technologies to control these factors has induced revolutionary development in the fields of sensors, catalysis, photonics, drug delivery, medical diagnostics, etc. [6-11]. While a considerable amount of research in these areas has been made with semiconductor nanoparticles (NPs), metal NPs have received relatively less attention. Of nanomaterials, Au NPs with a core diameter less than 3 nm have received more attention especially for electrochemical and optical sensors due to their unique properties, such as single-electron charging [12-15] and tunable highest occupied molecular orbital – lowest unoccupied molecular orbital (HOMO-LUMO) energy gap [13, 14]. In this size regime, ~10 to 250 atoms of Au are composed of the NP core and the surface of the NP core is protected by various organic molecules (e.g., thiols [16-19], amines [20-22], phosphines [23-25], etc.) to avoid decomposition or further aggregation of NPs. Such small Au NPs are well known to display size-dependent properties. In voltammetry, the transition from metal-like quantized double layer (QDL) charging to molecule-like redox charging is observed as the size of Au NPs decreases. For example, Au_{140} and Au_{225} NPs show QDL charging, while Au_{25}, Au_{55}, and Au_{75} NPs display redox charging [13-15, 26-28]. In addition, HOMO-LUMO energy gaps measured by voltammetry and electronic absorption spectroscopy become greater as the size decreases [12, 13]. These properties can also be tunable by varying the surface protecting ligands [14, 29-31]. The dependence of size and surface protecting ligands is interrelated, since the fraction of ligand-bonded surface Au atoms in the NP core increases as the core size decreases. Au NPs are good candidate materials to make a versatile platform for chemical and biological sensors, because (i) the adaptable functionalization toward selective and specific recognition of target analytes is possible on the surface of Au NPs, (ii) they provides surface-dependent properties, which can be utilized to accomplish the transduction of the binding event with target analytes, and (iii) the functionalized Au NPs may act as both molecular receptors and signal transducers on a sensor platform allowing to simplify the sensor design. In addition to these advantages, the molecule-like Au NPs (Au_{25} – Au_{75}) have several supplementary advantages. Compare with large Au NPs (> 3 nm diameter), the molecule-like Au NPs provides relatively high ratios of surface area to volume, allowing further amplification of signal, further enhancement of figures of merit, and further miniaturization of sensor platforms. Therefore, the molecule-like Au NPs are the more promising materials that can be directly applied to the research and development of sensors.

Although the size- and ligand-dependent properties of Au NPs have been studied extensively, they are still not fully understood especially for molecule-like Au NPs (Au_{25} – Au_{75}). In addition to this problem, the methods to control those properties and interrelation of size and surface-protecting ligands are not much investigated. Of various NP properties, we were interested in studying the optical properties of Au_{25} NPs. In this paper, we report how the optical properties (e.g., UV-Vis absorption and fluorescence) of Au_{25} NP are affected by their external environment, such as solvent.

II. EXPERIMENTAL SECTION

2.1. Chemicals

Tetrachloroauric acid trihydrate ($HAuCl_4{\cdot}3H2O$, > 99.99%), tetraoctylammonium bromide (TOA^+Br^-, 98%), 2-phenylethanethiol (PhC2SH, 98%), sodium borohydride ($NaBH_4$, ≥ 99%), benezne (99.8%), tetrahydrofuran (99.9%), 1,2-dichlorobenzene (99%), pyridine (99.8%), dichloroethane (99.8%), benzonitrile (99%), *N*,*N*-dimethylformamide (99.8%) were obtained from Sigma-Aldrich and used as received. Toluene, acetonitrile, methylene chloride, and methanol were purchased from Fisher Scientific (all Optima grade solvents). Deionized (DI) water (> 18 MΩ) produced from a Barnstead Fistreem II purification system was used in all syntheses and preparations.

2.2. Synthesis of Au_{25} Nanoparticles

Au_{25} NPs were synthesized by a modified version of the previously described method [16]. Briefly, $HAuCl_4{\cdot}3H_2O$ (3.1 g) was dissolved in DI water (100.0 mL) and phase-transferred to toluene (200.0 mL) in the presence of TOA^+Br^- (5.0 g). 3.5 mL of PhC2SH were added to react with $AuCl_4^-$ in toluene, forming a gold(I)-phenylethanethiol polymer. This material was reduced by fast addition of aqueous $NaBH_4$ (3.8 g in 50-mL ice-cold DI water), followed by vigorous stirring at 0°C. After 24 hours, the aqueous layer was discarded and toluene in the reaction mixture was removed with a rotary evaporator at room temperature. After the crude product was washed with a sufficient amount of methanol, $Au_{25}(SC2Ph)_{18}^-$ was extracted with acetonitrile. The purified $Au_{25}(SC2Ph)_{18}^-$ was confirmed by UV-Vis absorption spectroscopy, NMR, electrochemistry, and mass spectrometry. The chemical formula of the obtained Au_{25} NPs is $[TOA^+][Au_{25}(SC2Ph)_{18}^-]$.

2.3. UV-Vis Absorption and Near-IR (NIR) Photoluminescence Spectroscopy

UV-Vis absorption and NIR photoluminescence (PL) spectra were measured using a UV-1800 spectrophotometer (Shimadzu, Inc.) and a FL3-21 fluorometer (Horiba, Ltd.), respectively. The emission spectra were corrected for variation in the PMT spectral sensitivity. A quartz cuvette with 1-cm path length was used for the measurements of both absorption and NIR-PL spectra. The peak wavelengths (λ_{max}) of both absorption and photoluminescence of Au_{25} NPs are summarized in Table 1.

Table 1. λ_{max} of UV-Vis Absorption and Photoluminescence of Au_{25} Nanoparticles Measured in Various Solvents

Solvent	Absorption λ_{max} (nm)				Photoluminescence λ_{max} (nm)	
	Peak 1	Peak 2	Peak 3	Peak 4	Peak 1	Peak 2
$PhCH_3$	680	443	399	323	900	1052
Bz	682	443	399	324	901	1053
THF	681	445	399	321	-[a]	1082
ODCB	683	444	399	-[a]	901	1062
Py	684	443	398	-[a]	901	1068
DCM	682	446	399	324	-[a]	1079
DCE	680	443	397	322	-[a]	1070
PhCN	682	444	398	323	900	1054
DMF	682	444	398	323	-[a]	1078
MeCN	678	446	401	323	913	1030

a. Not observed.

III. RESULTS AND DISCUSSION

3.1. UV-Vis Absorption of Au_{25} NPs in Various Organic Solvents

The UV-Vis absorption spectra of Au_{25} NP were measured in 10 different organic solvents individually: toluene ($PhCH_3$), benzene (Bz), tetrahydrofuran (THF), 1,2-dichlorobenzene (ODCB), pyridine (Py), dichloromethane (DCM), 1,2-dichloroethane (DCE), benzonitrile (PhCN), *N*,*N*-dimethylformamide (DMF), acetonitrile (MeCN). Au_{25} NPs produced four absorption peaks at ~322, ~399, ~444, and 682 nm in most solvents we used (Table 1 and Fig. 1A). However, the peak at ~322 nm was not observed in ODCB and Py due to the cut-off regions of absorbance in those solvents. The HOMO-LUMO energy gap ($\Delta E_{H\text{-}L}$) was measured from the edges of absorption bands at ~682 nm. The estimated values of $\Delta E_{H\text{-}L}$ were 1.32 – 1.33 eV summarized in Table 2. This means that no change in the electronic structure of Au_{25} NPs occurred while they were dissolved in solvents used. The intensity of each absorption peak was linearly proportional to the concentration of Au_{25} NPs (Fig. 1B). This observation indicates that the dissolved Au_{25} NPs do not scatter UV-Vis light.

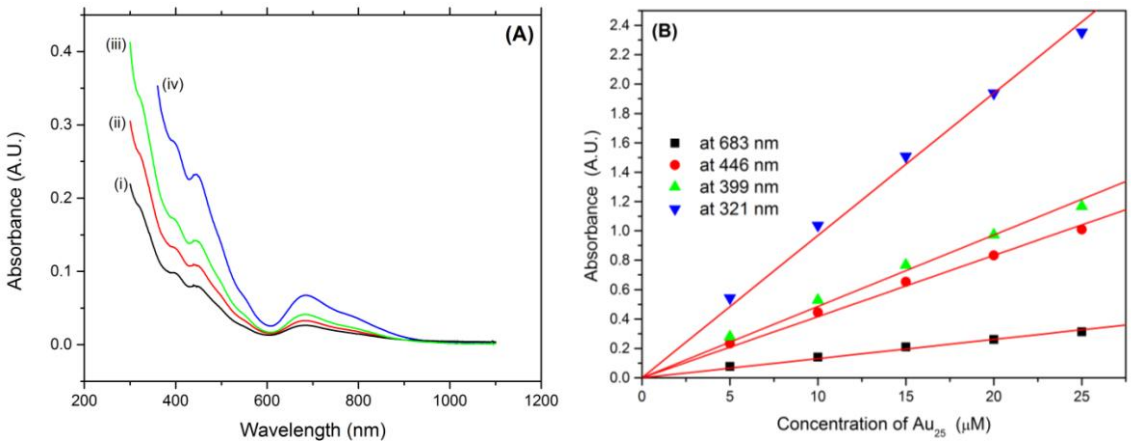

Figure 1. (A) UV-Vis absorption spectra of 3.0 μM Au_{25} NPs in (i) 1,2-dichloroethane (ii) toluene, (iii) benzonitrile, and (v) pyridine. (B) Plot of Absorbance vs. concentration obtained in dichloromethane.

Table 2. Summary of Normalized Empirical Parameters (E_T^N) of Solvent Polarity, HOMO-LUMO Energy Gap ($\Delta E_{H\text{-}L}$), and Molar Extinction Coefficients (ε) of Au_{25} NPs

Solvent	E_T^N [a]	$\Delta E_{H\text{-}L}$ (eV)	ε_1 ($M^{-1}cm^{-1}$)[b]	ε_2 ($M^{-1}cm^{-1}$)[c]	ε_3 ($M^{-1}cm^{-1}$)[d]	ε_4 ($M^{-1}cm^{-1}$)[e]
$PhCH_3$	0.099	1.32	1.52×10^4	5.11×10^4	6.09×10^4	1.21×10^5
Bz	0.111	1.33	1.52×10^4	5.10×10^4	6.02×10^4	1.20×10^5
THF	0.207	1.32	1.64×10^4	5.40×10^4	6.44×10^4	1.30×10^5
ODCB	0.225	1.33	2.28×10^4	7.75×10^4	9.08×10^4	-[f]
Py	0.302	1.33	1.83×10^4	6.20×10^4	7.26×10^4	-[f]
DCM	0.309	1.33	1.31×10^4	4.16×10^4	4.86×10^4	0.97×10^5
DCE	0.327	1.33	0.79×10^4	2.63×10^4	3.08×10^4	0.61×10^5
PhCN	0.333	1.33	1.63×10^4	5.52×10^4	6.59×10^4	1.30×10^5
DMF	0.404	1.32	1.22×10^4	4.07×10^4	4.73×10^4	0.93×10^5
MeCN	0.460	1.33	1.58×10^4	5.10×10^4	5.75×10^4	1.13×10^5

a. Taken from Ref. [32]. *b*. Measured at ~682 nm. *c*. Measured at ~444 nm. *d*. Measured at ~399 nm. *e*. Measured at ~322 nm. *f*. Not measurable due to the cut-off ranges of absorbance in solvent.

In order to measure the molar extinction coefficient (ε), five standard solutions of Au_{25} NPs were prepared using ten different solvents and UV-Vis absorbance was measured from these solutions. The ε values of Au_{25} dissolved in various solvents were determined from the slopes of plots of absorbance vs. concentration as shown in Figure 1B. The ε values measured at four different wavelengths are summarized in Table 2. Although there is an exception, Au_{25} NPs generally shows the higher ε in aromatic solvents ($PhCH_3$, Bz, ODCB, Py, and PhCN) than in non-aromatic solvents (THF, DCM, DCE, DMF, and MeCN). Since the surface of Au_{25} NPs are protected with 2-phenylethanethiols (aromatic thiols), they would be better solvated with aromatic solvents than non-aromatic solvents. Therefore, the excited state of Au_{25} NPs could be better stabilized. The obtained ε was correlated with the normalized empirical parameters (E_T^N) of solvent polarity, which were derived from the long-wavelength UV-Vis charge transfer absorption band of the negatively solvatochromic pyridinium N-phenolate betaine dyes measured at 25 °C [32]. As shown in Fig. 2, the ε values of Au_{25} NPs decreased as solvent polarity increased (E_T^N increased).

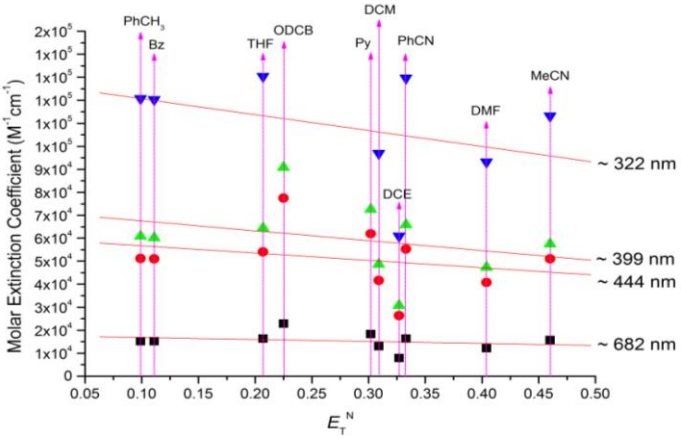

Figure 2. Dependence of the molar extinction coefficients of Au_{25} nanoparticles on the normalized empirical parameters (E_T^N) of solvent polarity. ~322, ~399, ~444, and ~682 nm are λ_{max} for absorption peak 4, 3, 2, and 1, respectively.

3.2. Photoluminescence of Au_{25} NPs in Various Organic Solvents

As shown in Fig. 3, Au_{25} NPs produced NIR PL at ~1080 nm when they were excited at 400 nm. In aromatic solvents, they displayed an additional shoulder-like band at ~900 nm (Fig. 3). The wavelengths of PL peaks measured from various organic solvents are summarized in Table 1. Our results are quite similar to the previously reported results [14].

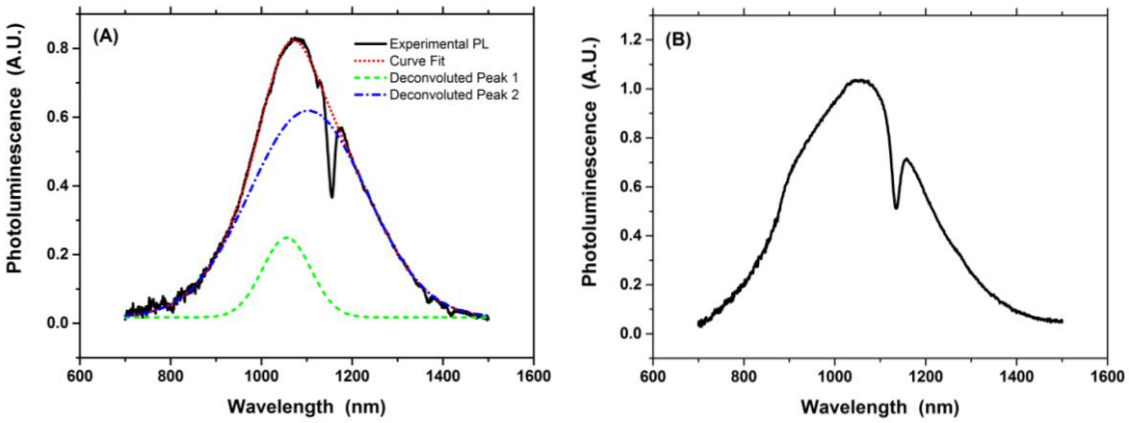

Figure 3. Photoluminescence spectra of 3 μM Au_{25} nanoparticles dissolved in (A) dichloromethane and (B) benzonitrile. In (A), Gaussian curve fit and deconvoluted PL peaks are also shown.

The major PL peak at 1080 nm was resulted from the surface-state emission, while the additional shoulder-like band at ~900 nm was from the localized surface-state emission generated by solvation with aromatic solvents. Gaussian curve fitting was performed to deconvolute these attributions (core-state vs. surface-state emissions, Fig. 3A). From the excited state of Au_{25} NPs, two emission processes (core-state and surface-state) compete one another. The core-state emission process seems to be always dominant in all organic solvents we used, but the surface-state emission process is still strong enough to observe additional emission in aromatic solvents.

The relative quantum efficiency (Φ_R) for PL of Au_{25} NPs dissolved in various organic solvents were measured using Q-switch 5 as a reference dye, whose quantum efficiency (Φ) is 1.667×10^{-4} in DCE [33]. The estimated Φ_R values are summarized in Table 3. Φ_R was greater when Au_{25} NPs was excited by the excitation wavelength (λ_{ex}) of 400 nm rather than 675 nm (Table 3). In order to investigate the effect of solvent polarity on PL, Φ_R was correlated with E_T^N (Fig. 4). Unlike UV-Vis absorption, Φ_R of Au_{25} NPs was more significantly affected by aromatic solvents than non-aromatic solvents (Fig. 4). Φ_R of Au_{25} NPs was almost independent of E_T^N for non-aromatic solvents (Fig. 4B).

Table 3. Relative Quantum Efficiency (Φ_R) for Photoluminescence of Au_{25} NPs Dissolved in Various Organic Solvents

Solvent	$PhCH_3$	Bz	THF	ODCB	Py	DCM	DCE	PhCN	DMF	MeCN
$\Phi_{R,1}$ ($\times 10^{-3}$)[a]	10.7	12.2	10.2	10.3	11.1	9.7	7.6	9.2	9.0	10.8
$\Phi_{R,2}$ ($\times 10^{-3}$)[b]	19.6	20.4	13.4	16.4	16.6	13.2	13.7	18.5	14.5	15.8

a. Determined with λ_{ex} = 675 nm. *b*. Determined with λ_{ex} = 400 nm.

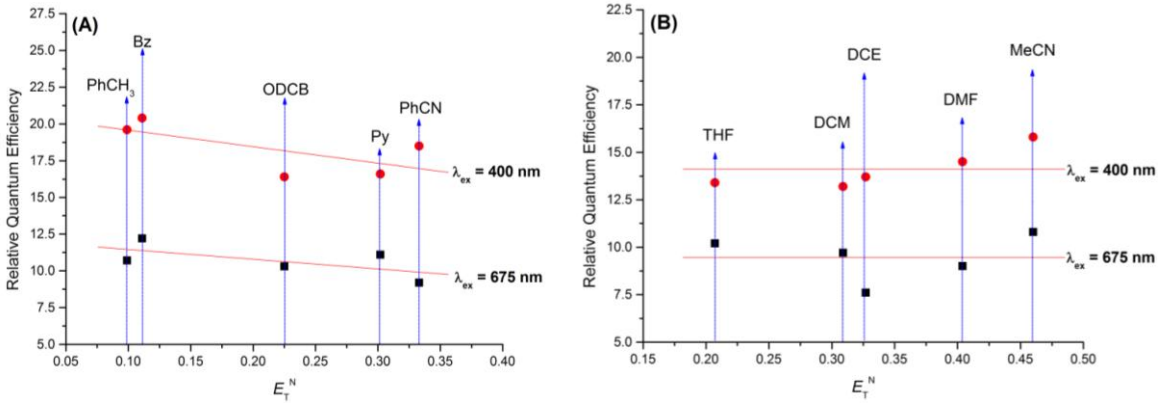

Figure 4. Dependence of relative quantum efficiency of Au_{25} NPs, dissolved in (A) aromatic solvents and (B) non-aromatic solvents, on the normalized empirical parameters (E_T^N) of solvent polarity.

IV. CONCLUSION

The optical properties of Au_{25} NPs were strongly affected by the polarity of solvents, where they were dissolved in. Although there were a few exceptions, the molar extinction of Au_{25} NPs was observed to decrease roughly as the solvent polarity increases. In addition, the higher values of the molar extinction was measured in aromatic solvents than in non-aromatic solvents. However, the HOMO-LUMO energy gap of Au_{25} NPs was almost constant (1.32 – 1.33 eV), indicating that the electronic structure of Au_{25} NPs was not affected by various solvent but the stability of NP's excited states was. The shape of PL spectra was different depending on the type of solvents (aromatic vs. non-aromatic). The aromatic solvents generated an additional shoulder-like PL band at ~900 nm in addition to the major peak at ~1100 nm, while non-aromatic solvents showed the major PL peak only. Depending on λ_{ex}, the PL intensity was variable but the wavelength of a PL peak was constant. The Φ_R for the PL of Au_{25} NPs was linearly decreased with increasing E_T^N for aromatic solvents ($PhCH_3$, Bz, ODCB, Py, and PhCN). However, Φ_R was almost independent of E_T^N for non-aromatic solvents (THF, DCM, DCE, DMF, and MeCN).

ACKNOWLEDGEMENTS

It is gratefully acknowledged that this research was supported in part by grants from Research Corporation (CCSA10523), CSU Program for Education & Research in Biotechnology, Faculty-Sponsored Student Research Award.

REFERENCES

[1] G. Hodes, When Small Is Different: Some Recent Advances in Concepts and Applications of Nanoscale Phenomena, Advanced Materials, 19(5), 2007, 639-655.
[2] G. Schmid, Nanoparticles: From Theory to Application (Weinheim, Germany: Wiley-VCH, 2004).
[3] M.A. El-Sayed, Small Is Different: Shape-, Size-, and Composition-Dependent Properties of Some Colloidal Semiconductor Nanocrystals, Accounts of Chemical. Research, 37(5), 2004, 326-333.
[4] P.C. Ray, Size and Shape Dependent Second Order Nonlinear Optical Properties of Nanomaterials and Their Application in Biological and Chemical Sensing, Chemical Reviews, 110(9), 2010, 5332-5365.
[5] R.A. Andrievskii and A.V. Khachoyan, Role of Size-Dependent Effects and Interfaces in Physicochemical Properties of Consolidated Nanomaterials, Russian Journal of General Chemistry, 80(3), 2010, 555-566.
[6] Y.-W. Lin, C.-C. Huang, and H.-T. Chang, Gold Nanoparticle Probes for the Detection of Mercury, Lead, and Copper Ions, Analyst, 136(5), 2011, 863-871.
[7] F. Wang and S. Hu, Electrochemical Sensors Based on Metal and Semiconductor Nanoparticles, Microchimica Acta, 165(1), 2009, 1-22.
[8] B.K. Min and C.M. Friend, Heterogeneous Gold-Based Catalysis for Green Chemistry: Low-Temperature CO Oxidation and ropene Oxidation, Chemical Reviews, 107(6), 2007, 2709-2724.
[9] N.L. Rosi and C.A. Mirkin, Nanostructures in Biodiagnostics, Chemical Reviews, 105(4), 2005, 1547-1562.
[10] P.K. Jain, X. Huang, I.H. El-Sayed, and M.A. El-Sayed, Noble Metals on the Nanoscale: Optical and Photothermal Properties and Some Applications in Imaging, Sensing, Biology, and Medicine, Accounts of Chemical Research, 41(12), 2008, 1578-1586.
[11] J.M. Campelo, D. Luna, R. Luque, J.M. Marinas, and A.A. Romero, Sustainable Preparation of Supported Metal Nanoparticles and Their Applications in Catalysis, ChemSusChem, 2(1), 2009, 18-45.
[12] R.W. Murray, Nanoelectrochemistry: Metal Nanoparticles, Nanoelectrodes, and Nanopores, Chemical Reviews, 108(7), 2008, 2688-2720.
[13] S. Chen, R.S. Ingram, M.J. Hostetler, J.J. Pietron, R.W. Murray, T.G. Schaaff, J.T. Khoury, M.M. Alvarez, and R.L. Whetten, Gold Nanoelectrodes of Varied Size: Transition to Molecule-Like Charging, Science, 280(5372), 1998, 2098-2101.
[14] D. Lee, R.L. Donkers, G. Wang, A.S. Harper, and R.W. Murray, Electrochemistry and Optical Absorbance and Luminescence of Molecule-like Au38 Nanoparticles, Journal of the American Chemical Society, 126(19), 2004, 6193-6199.
[15] B.M. Quinn, P. Liljeroth, V. Ruiz, T. Laaksonen, and K. Kontturi, Electrochemical Resolution of 15 Oxidation States for Monolayer Protected Gold Nanoparticles, Journal of the American Chemical Society, 125(22), 2003, 6644-6645.
[16] M. Brust, M. Walker, D. Bethell, D.J. Schiffrin, and R. Whyman, Synthesis of Thiol-Derivatised Gold Nanoparticles in a Two-Phase Liquid-Liquid System, Journal of the Chemical Society, Chemical Communications, 1994, 801-802.
[17] R.L. Donkers, D. Lee, and R.W. Murray, Synthesis and Isolation of the Molecule-like Cluster $Au_{38}(PhCH_2CH_2S)_{24}$, Langmuir, 20(5), 2004, 1945-1952.
[18] R.L. Whetten, M.N. Shafigullin, J.T. Khoury, T.G. Schaaff, I. Vezmar, M.M. Alvarez, and A. Wilkinson, Crystal Structures of Molecular Gold Nanocrystal Arrays, Accounts of Chemical Research, 32(5), 1999, 397-406.
[19] A.C. Templeton, W.P. Wuelfing, and R.W. Murray, Monolayer-Protected Cluster Molecules, Accouts of Chemical Research, 33(1), 2000, 27-36.
[20] D.V. Leff, L. Brandt, and J.R. Heath, Synthesis and Characterization of Hydrophobic, Organically-Soluble Gold Nanocrystals Functionalized with Primary Amines, Langmuir, 12(20), 1996, 4723-4730.
[21] L.O. Brown and J.E. Hutchison, Controlled Growth of Gold Nanoparticles during Ligand Exchange, Journal of the American Chemical Society, 121(4), 1999, 882-883.
[22] S. Gomez, K. Philippot, V. Collière, B. Chaudret, F. Senocq, and P. Lecante, Gold Nanoparticles from Self-Assembled Gold(I) Amine Precursors, Chemical Communications, 2000, 1945-1946.
[23] G. Schmid, Large Clusters and Colloids. Metals in the Embryonic State, Chemical Reviews, 92(8), 1992, 1709-1727.
[24] W.W. Weare, S.M. Reed, M.G. Warner, and J.E. Hutchison, Improved Synthesis of Small ($d_{CORE} \approx 1.5$ nm) Phosphine-Stabilized Gold Nanoparticles, Journal of the American Chemical Society, 122(51), 2000, 12890-12891.
[25] J. Petroski, M.H. Chou, and C. Creutz, Rapid Phosphine Exchange on 1.5-nm Gold Nanoparticles, Inorganic Chemistry, 43(5), 2004, 1597-1599.
[26] R.L. Wolfe and R.W. Murray, Analytical Evidence for the Monolayer-Protected Cluster $Au_{225}[(S(CH_2)_5CH_3)]_{75}$, Analytical Chemistry, 78(4), 2006, 1167-1173.

[27] R.L. Stiles, R. Balasubramanian, S.W. Feldberg, and R.W. Murray, Anion-Induced Adsorption of Ferrocenated Nanoparticles, Journal of the American Chemical Society, 130(6), 2008, 1856-1865.
[28] R. Balasubramanian, R. Guo, A.J. Mills, and R.W. Murray, Reaction of $Au_{55}(PPh_3)_{12}Cl_6$ with Thiols Yields Thiolate Monolayer Protected Au_{75} Clusters, Journal of the American Chemical Society, 127(22), 2005, 8126-8132.
[29] R. Guo and R.W. Murray, Substituent Effects on Redox Potentials and Optical Gap Energies of Molecule-like $Au_{38}(SPhX)_{24}$ Nanoparticles, Journal of the American Chemical Society, 127(34), 2005, 12140-12143.
[30] G.H. Woehrle, M.G. Warner, and J.E. Hutchison, Ligand Exchange Reactions Yield Subnanometer, Thiol-Stabilized Gold Particles with Defined Optical Transitions, The Journal of Physical Chemistry B, 106(39), 2002, 9979-9981.
[31] S. Knoppe, I. Dolamic, T. Bürgi, Racemization of a Chiral Nanoparticle Evidences the Flexibility of the Gold–Thiolate Interface, Journal of the American Chemical Society, 134(31), 2012, 13114-13120.
[32] C. Reichardt, Solvatochromic Dyes as Solvent Polarity Indicators, Chemical Reviews, 94(8), 1994, 2319-2358.
[33] A. Seilmeier, B. Kopainsky, and W. Kaiser, Infrared Fluorescence and Laser Action of Fast Mode-Locking Dyes, Applied Physics, 22(4), 1980, 355-359.

Amit Patel. "Optical Properties of Molecule-Like Au25 Nanoparticles." International Journal of Engineering Science Invention (IJESI), vol. 6, no. 9, 2017, pp. 71–76.